

Slope Stability Assessment and Landslide Susceptibility Map Production of Wadi Dhahr Area, Northwest of Sana'a, Yemen

Adnan A. Barahim^{1*}, Khaled M. Khanbari^{1,2}, Amal F. Algodami¹, Ziad A. Almadhaji³ and Ahmed M. Adris².

¹ Department of Earth and Environmental Science, Faculty of Science, Sana'a University, Sana'a, Yemen; ² Yemen Remote Sensing and GIS Center; ³ Geological Survey and Mineral Resources Board (GSMRB). *Email: barahimadnan@gmail.com.

ABSTRACT: A slope stability assessment of Wadi Dhahr area, located northwest of Sana'a the capital of Yemen, was carried out in this study. The study area consists of sandstone and volcanic rocks that are deformed by number of faults, joints and basaltic dykes. All the important factors affecting slope stability in the area such as slope angle, slope height, discontinuities measurements, weathering, vegetation cover, rainfall and previous landslides were evaluated. The study was conducted based on the integration of field investigation and satellite image processing. A landslide susceptibility map was produced with the Landslide Possibility Index (LPI) System, and the correlation values were computed between the factors measured and Landslide Possibility Index values. The fractures counted by satellite image were categorised according to their length and zones based on their concentrations. It was found that plain sliding and rockfall are the main modes of failure in the area, while rolling and toppling are rare. Some remedial measures are proposed to protect the slopes where it is needed, such as the removal of rock overhangs, unstable blocks and trees, and by supporting the toe of slopes and overhanging parts by retaining walls and erecting well sealed drainage conduits. The results will assist in slope management and land use planning in the area.

Keywords: Landslide; LPI; Susceptibility Map; Structure; Wadi Dhahr; Yemen.

تقييم إستقرارية المنحدرات و إنتاج خارطة القابلية للانهيارات الارضية لوادي ظهر شمال غرب صنعاء – اليمن

عدنان عبدالعزيز بارحيم، خالد محمد خنبري، امل فيصل القديمي، زياد احمد المدحجي و احمد محمد إدريس

المخلص: تم اجراء تقييم إستقرارية المنحدرات لمنطقة وادي ظهر شمال صنعاء عاصمة اليمن. تتكون منطقة الدراسة من الصخور الرملية و البركانية، متأثرة بعدد من الفواصل و الفوالق و القواطع البازلتية. جميع العوامل المهمة المؤثرة في إستقرارية المنحدرات في المنطقة مثل زاوية المنحدر، ارتفاع المنحدر، قياسات الانقطاعات، التجوية، الغطاء النباتي، السقوط المطري و الانهيارات السابقة تم تقييمها. اعتمدت الدراسة على تكامل التحري الحقل مع معالجة المرئيات الفضائية. خارطة القابلية للانهيارات الارضية انتجت بنظام دليل احتمالية الانهيارات الارضية، قيم الارتباط حسبت بين كل العوامل المقاسة و قيم دليل احتمالية الانهيارات الارضية. حسبت التشققات من خلال المرئية الفضائية و تم تصنيفها وفق اطوالها و اتجاهاتها وكذلك تنطبقها على اساس كثافتها. وجد ان الانزلاق المستوي و السقوط الصخري يمثلان النمطين الشائعين، في حين ان الدرجة و الانقلاب نادرين. كما تم اقتراح عدد من المعالجات لحماية المنحدرات عند الحاجة مثل ازالة الصخور المعلقة، الكتل غير المستقرة و الاشجار. تدعيم قدم المنحدر و الاجزاء المعلقة بالجدران الساندة و عمل قنوات تصريف محكمة التبتين. نتائج الدراسة تفيد في ادارة مخاطر المنحدرات و تخطيط استخدام الارض في المنطقة.

الكلمات المفتاحية: انزلاقات ارضية، خارطة قابلية الانهيارات الارضية، تراكيب، وادي ظهر، اليمن.



1. Introduction

Landslides caused by Massive Rock Slope Failure (MRSF) are the major geological hazard in many parts of the world and have been responsible for some of the most destructive natural disasters of recent history [1]. Landslides resulting from large-scale rock slope failures are the major hazard in mountainous regions. In the 20th century, disasters caused by massive rock slope failures killed more than 50,000 people on a global basis [2].

Landslide susceptibility can be defined as the probability of the occurrence of a landslide based on the relationship between the occurrence distribution and a set of predisposing factors, i.e. geo-environmental thematic variables in the area [3, 4]. A landslide susceptibility map depicts areas likely to have landslides in the future by correlating some of the principal factors that contribute to landslides with the past distribution of slope failures [3, 5].

Therefore, landslide susceptibility maps represent a powerful tool since they provide coherent information on potentially unstable slopes [6]. It is an important step prior to landslide assessment planning, management and disaster mitigation [7 and 8]. In this context, the landslide susceptibility assessment can be considered the initial step towards the landslide hazard and risk assessment and the end product in land-use planning and environmental impact assessment, as well as an important tool in early warning system techniques [9, 10].

Remote sensing and Geographic Information System (GIS) techniques are useful for landslide susceptibility mapping and can help identify the areas best suited for developmental activities [11, 12, 13]. Remote sensing data provides quality, high resolution information on various terrain parameters such as geology, liniment, drainage, slope and land use / land cover. For this study, these parameters were collected, processed and constructed into a spatial database using GIS.

The western part of Yemen is a mountainous region, and much MRSF has been recorded in the region, this frequently being exacerbated by the expansion of human activities (such as unsuitable patterns of drainage of sewage and unstudied slope cutting).

The objective of this study is to evaluate fractures control and rock slope stability, and generate a landslide susceptibility map of the Wadi Dhahr area.

2. Study area

The study was conducted within the Wadi Dhahr area (19.640 Km²), which is located in the western part of Yemen, 12 km to the northwest of Sana'a city, capital of Yemen (Figure 1). Wadi Dhahr is a U-shaped wadi in a mountainous area with a cold dry climate. The annual average temperatures range between -6 to 37 °C and the annual precipitation ranges between 100-500 mm/year [14] with considerable (32.36%) vegetative cover. The wadi contains an archeological village, with one of the most important monumental tourist sites, which is known as Dar Al Hajar palace (Figure 2).

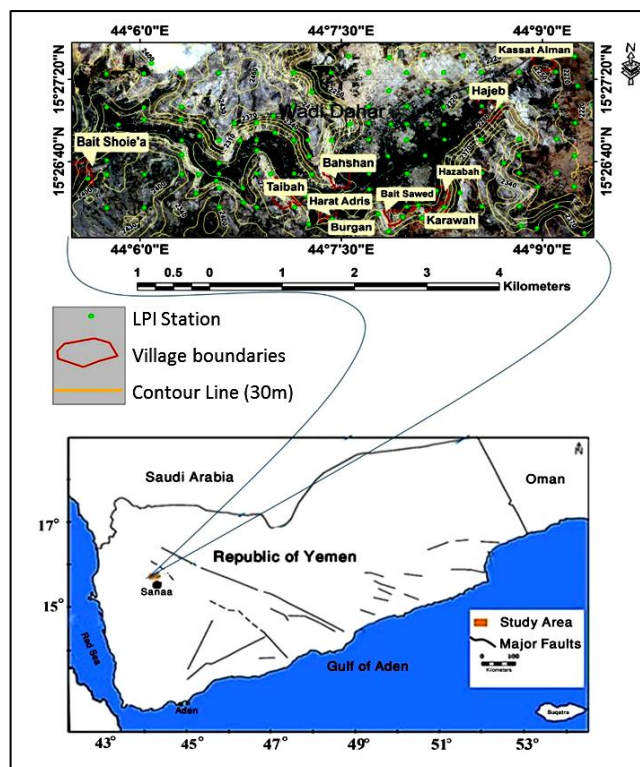


Figure 1. Location and topographic map of the study area.



Figure 2. Dar Al Hajar (stone house) monument and the slopes surrounding Wadi Dhahar.

3. Geologic setting

Wadi Dhahr is located in the western part of Yemen, which is characterized mainly by Cenozoic Volcanics (Tertiary and Quaternary Volcanics), granitic intrusion and some outcrops of Mesozoic sedimentary rocks (Cretaceous Sandstone and Jurassic Limestone) overlying the Precambrian basement rocks [15,16]. The geology of the study area is characterized mainly by Cenozoic Volcanics (Tertiary and Quaternary Volcanics) and Cretaceous sandstone.

The geological map produced by the processing and interpretation of the Landsat-7 (ETM) Image dated 2016 (Figure 3) shows that the Cretaceous sandstones (Tawilah Group) outcrop dominantly in the Wadi Dhahr area. This rock unit represents the oldest rock unit in the study area. The Tawilah Group is composed almost entirely of sandstones and conglomerates. The upper formation of the Tawilah Group contains shallow marine sandstone [17]. The general dip of Cretaceous sandstones is nearly horizontal [18]. The Tawilah Group is intruded by basaltic dykes and overlain by Tertiary and Quaternary volcanics, which are related to the emplacement of the Afar hotspot since the Oligocene [19, 20]. Structural analysis confirms that there is a strong link between volcanic activity and extension and that the evolution of the volcanic margin is closely related to the Afar plume [20, 21]. Recent alluvium deposits cover the base of the wadi.

The Wadi Dhahr area is affected mainly by normal and oblique faults and joints which are associated with the opening of the Red Sea and Gulf of Aden since the Oligo-Miocene [18]. The geological map (Figure 3) shows that the study area is affected by major structures trending NW-SE, N-S and ENE-WSW. These trends correspond to the major faults that affect the western part of Yemen [18, 20, 21, 22, 23].

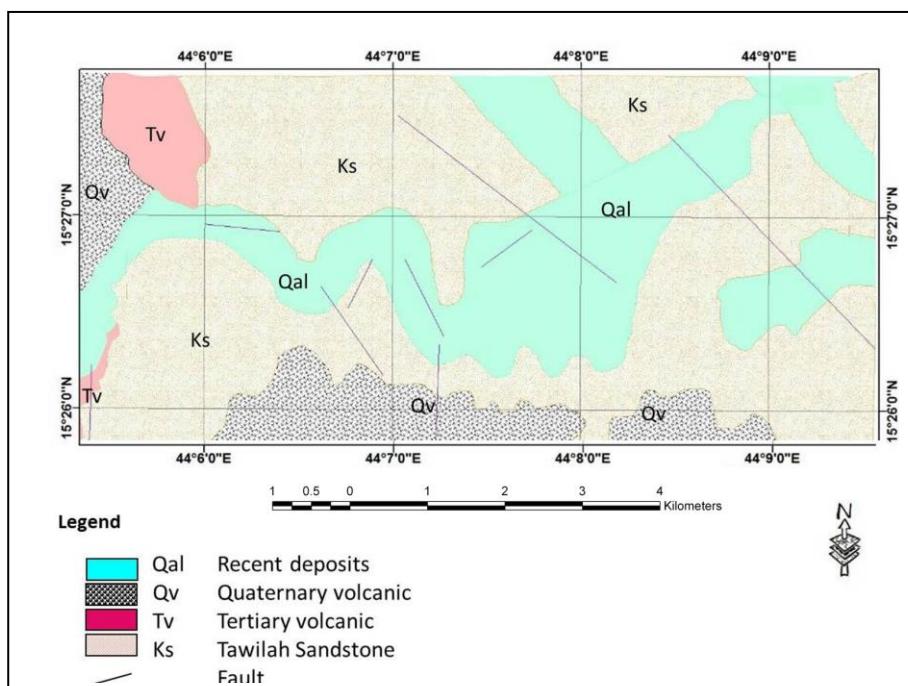


Figure 3. Geological map for the study area based on a Landsat-7 satellite image.

4. Methodology

Remote Sensing and GIS techniques were used to study fracture control and slope stability hazards which affect the Wadi Dhahr area. Remote sensing data included a Landsat-7 (ETM) image, a high resolution Quick-Bird image with 60cm resolution dated 2016 (source: Google Earth) and an STRM Digital Elevation Model (DEM) with 30m resolution. These data were provided by the Yemen Remote Sensing and GIS Center (YRSC).

The Landsat ETM image was processed and interpreted to produce a geological map of the study area, while the high resolution image was mainly used to detect all the fractures, using a visual technique. Both the Landsat and high resolution images were used to produce a land use/cover map of the study area. Additionally, DEM was used to produce a slope map.

The field data was collected over a period of fourteen days with the Geological Survey and Mineral Resources Board (GSMRB) staff. The main features affecting slope stability were measured and estimated in the field at 152 stations (locations) within area of 19.640 km². These included slope height (the vertical distance between the top and the toe of the slope at the station), slope angle, grade of fracture, grade of weathering, gradient of discontinuities, spacing of discontinuities, orientation of discontinuities, vegetation cover, water infiltration and previous landslide. Then the parameters were integrated using a heuristic method [24, 25] as a rating system according to the Landslide Possibility Index chart (LPI) [26, 27] (Figure 4); this is similar to an Analytical Hierarchy Process (AHP) approach, which is a multi-objective, multi-criteria decision-making approach that enables the user to arrive at a scale of preferences drawn from a set of alternatives [28,29,30, 31]. The correlation coefficient values between each factor and LPI value were computed by Microsoft excel software in order to understand which factors significantly affect slope instability in the study area.

Landslide Possibility Index (LPI)							
No.	Factor	Scale	Estimation	No.	Factor	Scale	Estimation
1	SLOPE HEIGHT (M)	1 - 8 m	1	2	SLOPE ANGLE (°)	< 15°	0
		9 - 15 m	2			15° - 30°	1
		16 - 25 m	3			30° - 45°	2
		26 - 35 m	4			45° - 60°	3
		> 35 m	5			> 60°	4
3	GRADE OF FRACTURE (Number of Fracture)	Sound	0	4	GRADE OF WEATHERING (Alteration and compressive strength)	Fresh	0
		Moderately Fractured	1			Slightly Weathered	1
		Highly Fractured	2			Moderately Weathered	2
		Completely Fractured	3			Highly Weathered	3
						Completely Weathered	4
5	GRADIENT OF THE DISCONTINUITIES (°)	< 15	0	6	SPACING OF THE DISCONTINUITIES (M)	3 <	0
		15° - 30°	1			3 - 1	1
		30° - 45°	2			1 - 0.3	2
		45° - 60°	3			0.3 - 0.05	3
		> 60°	4			0.05 >	4
7	ORIENTATION OF THE DISCONTINUITIES	Favourable	0	8	VEGETATION COVER (%)	Void (< 20%)	0
		Unfavourable	4			Scarce (20% - 60%)	1
9	WATER INFILTRATION (mm/year)	Inexistent	0	10	PREVIOUS LANDSLIDES (m ² /year)	Not registered	0
		Scarce	1			Registered Small volume (< 3m ³ /year)	1
		Abundant (>500mm/year) Permanent	2			Registered High volume (> 3m ³ /year)	2
		Abundant (>500mm/year) Seasonal	3				

1 + 2 + 3 + 4 ± 5 + 6 + 7 + 8 + 9 + 10 = LPI value									
The LPI value is obtained by adding the estimations of attributes 1 to 10. If the orientation of the discontinuities is favourable, subtract the estimation of the gradient.									
I (Nil) (0-5)		III (Moderately low) (11-15)		V (High) (21-25)					
II (Low) (6-10)		IV (Moderately high) (16-20)		VI (Very high) (>25)					

Figure 4. LPI chart used in the study [26,27].

All interpretations of remote sensing data and field data were implemented in ArcGIS 10.2 in order to evaluate the fractures and slope instability, and to produce the landslide susceptibility map.

In addition to the 152, ten stations were measured within greater detail by using remote sensing data (fracture orientation order and density) and field investigation (of specific slope attitude, structure, failure type, probability and causes) in order to study structure and failure modes and causes.

The engineering characteristics of the rock mass were described according to the Geological Society of London Engineering Group Working Party [32]. The relationships between slope faces and bed attitude were classified according to Al-Saadi's slope classification [33].

In this study, a kinematic analysis was implemented to determine the type and probability of failure using Rock Pack III computer program. A kinematic analysis method, which was first described by Hoek and Bray [34], developed by Goodman [35] and modified by Wyllie and Mah [36], allows the investigation of potential planar, wedge and toppling failure modes of rock slopes [37]. The inclination of slope (or dip of structure) is indicated by two numbers, the one to the left (three digits) represents the slope (or dip) direction and the one to the right (two digits) represents the slope (or dip) angle. The symbol (OH) is used for overhanging slopes (for example, 080°/58°- OH°).

5. Land use/cover

A land use/cover map was created to describe the differences in human activities and in the actual surface covering of the land within the study area. Figure 5 represents the distribution of the various surface activities in the study area. Visual interpretation of the Landsat ETM and high resolution image showed that lithological outcrops cover 19% of the area, and that the built areas (with a population of 90,381) cover 15.25% and that they are located close to the slopes. The agricultural zones (grapes, coffee and kat) are significant, covering 32.36% of the area. Pastureland covers 33.41%, the greatest area. Asphaltic and paved roads are represented in the map by lines.

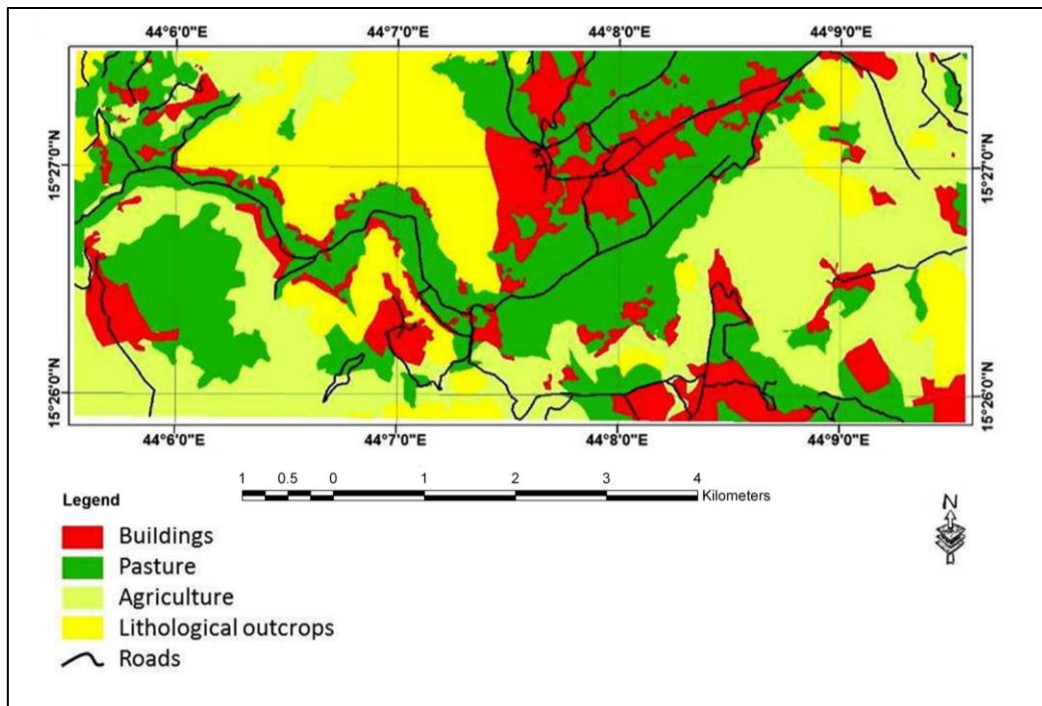


Figure 5. Land use/cover map for the study area, extracted from a high resolution (60 cm) Satellite image by Google Earth- 2016.

6. Fractures analysis

The direction, length and density of fractures affect the mode and the extent of failure in terms of slope stability [34 and 36]. Structural and topographical geology maps can be used to facilitate the planning of geohazard mitigation [31]. Visual interpretation techniques of the high resolution satellite image (60 cm) were used for detecting fractures (faults and joints), and for producing a fracture map (Figure 6). The identified fracture map includes 2990 fractures. Most of these fractures are affecting the Cretaceous sandstone.

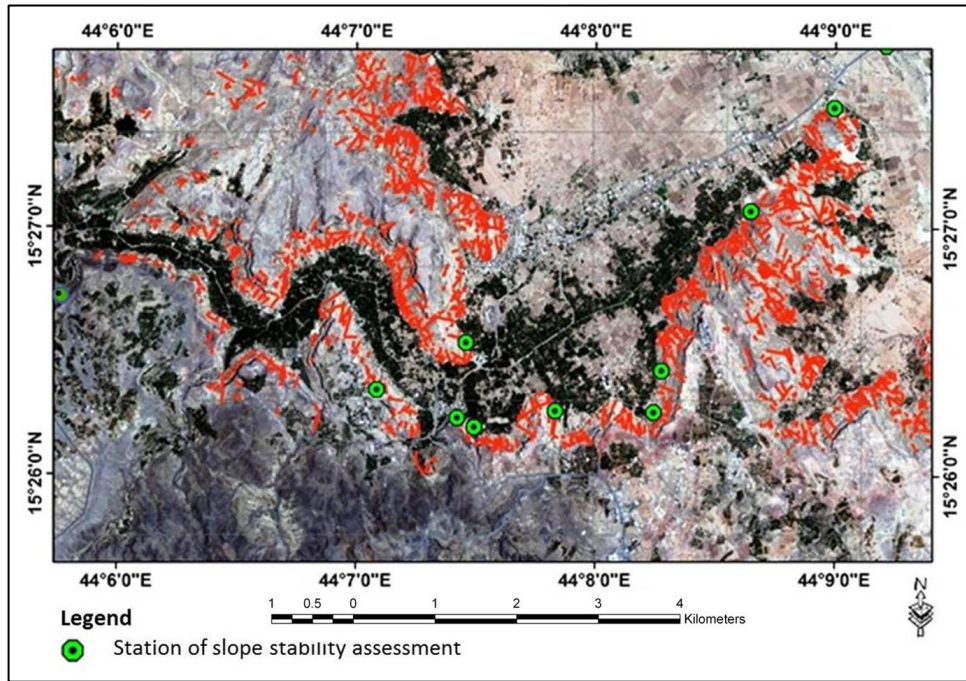


Figure 6. Fracture distribution from a Landsat-7 high resolution satellite image (15 cm) for the study area.

- **Fracture Orientation Analysis**

Fractures are graphically represented in a rose-diagram (Figure 7) based on the number of fractures. The rose-diagram shows that the dominant trends of the fractures are: NW-SE, NNW-SSE, N-S, NNE-SSW and NE-SW. Some other trends: ENE-WSW, E-W and WNW-ESE were observed but are less frequent.

The measured fractures in general are nearly subvertical. They were classified based on the azimuth of the strike direction into eight sets. Table 1 shows the number and percentage of fractures in each set.

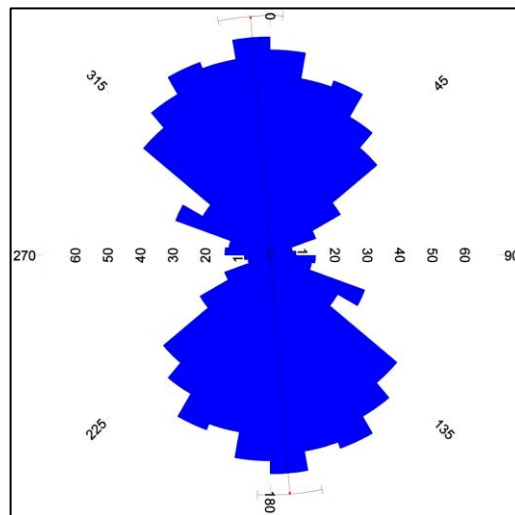


Figure 7. Rose diagram showing the general orientation of discontinuities in the study area.

Table 1. Number and percentage of the fractures for each set of orientation.

Direction (°)	0-22.5	>22.5 - 45	>45 - 67.5	>67.5 - 90	>90 - 112.5	>112.5 - 135	>135 - 157.5	>157.5 - 180	total
Number of fractures	537	499	239	151	188	306	495	575	2990
Percentage	17.96	16.69	7.99	5.05	6.29	10.23	16.56	19.23	100

- *Fracture Length Analysis:*

The fractures were divided into 6 classes according to their length. Table 2 shows the number and percentage of fractures in each class. The orientation of fractures and their length was established to define the length range for each trend (Figure 8, Table 2). The results show that the NNE-SSW, NNW-SSE and N-S trending sets are the most frequent, with a wide range of lengths.

Table 2. Number, percentage, and orientation of fractures

Length (m)	A 0 - 20	B >20 -40	C >40- 60	D >60-80	E >80- 100	F >100	total
Number	1612	703	334	162	79	100	2990
%	53.9	23.5	11.2	5.4	2.6	3.3	100
dominant trend	NW-SE	NNW-SSE	NNE-SSW	NNE-SSW	NNW-SSE	NW-SE	NW-SE to NNE-SSW
second trend	NNE-SSW	NW-SE	N-S	N-S	NE-SW	E-W	NE-SW to NNE-SSW

- *Fracture Density Analysis:*

The fracture density map shows that the highest fracture density was recorded in the north, east and central parts of the study area close to the occurrence of faults (Figure 9). The fractures mainly affect the Cretaceous sandstones, while the volcanic rocks show a very low density of fractures. There is no significant record of fractures in the wadi deposits. The density of fractures is related to the tectonic setting and the physical properties of the rock units of the study area [18].

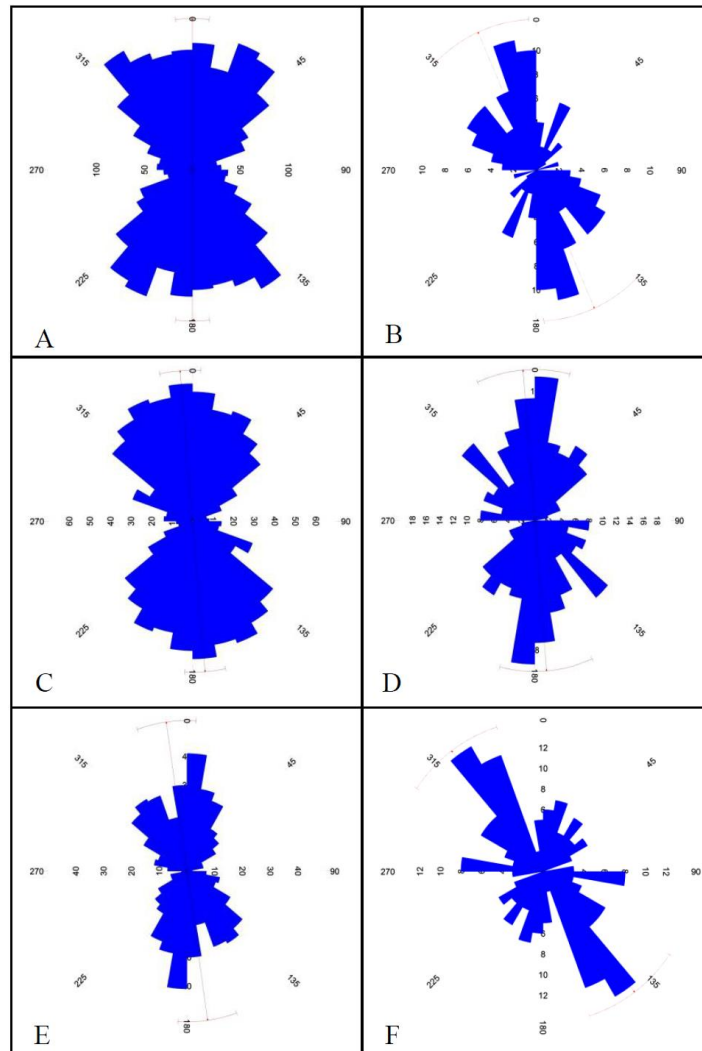


Figure 8. Rose diagrams showing the relationship between trends and lengths of fractures, for classes from A to F (see Table 2).

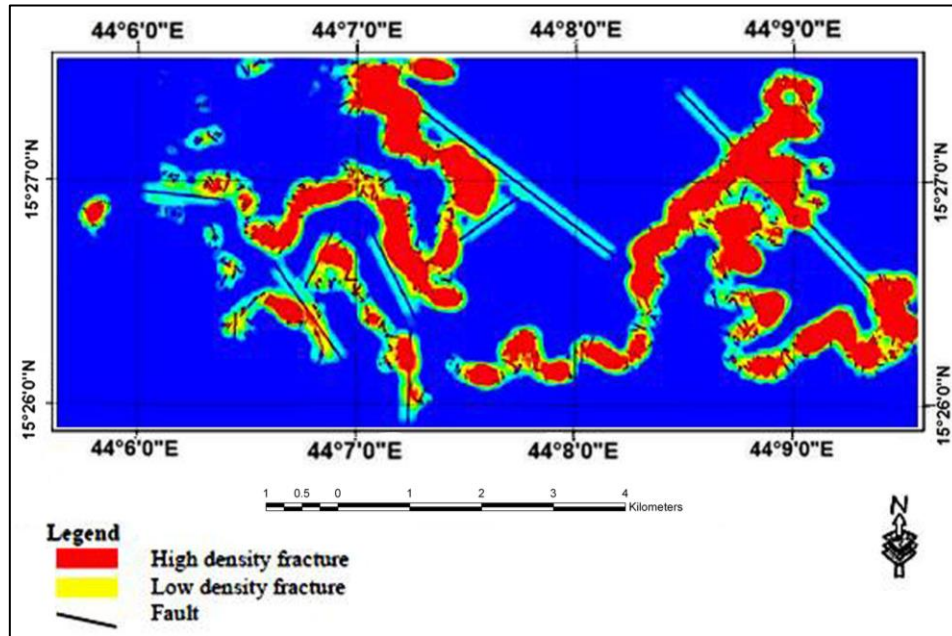


Figure 9. Fracture density for the study area.

7. Landslide data analysis, results and discussion

7.1 Aspects of failures

Detailed studies for slope stability assessment were conducted at ten stations, to representatively sample failures at village slopes within the wadi. (each station has a circular area of about 100 m diameter) (Figure 10). Stations 2 to 10 are located in a Tawilah group, with an average trend of $220^{\circ}/07^{\circ}$. According to the Geological Society Engineering Group Working Party of London [30] the rock units identified are of yellowish red colour and medium grain size, medium bedded, with widely spaced joints, slightly weathered, gravely sandstone, which is moderately permeable with strong compressive strength characterized by semi vertical dykes. Station 1 lies on basaltic rock identified as of black colour and fine grain size, thick bedded to bulky, moderately to widely spaced joints, slightly weathered, vesicular basalt, which is moderately permeable and has very strong compressive strength.

The kinematic analysis method which was implemented in the study assumes that the shear strength of the sliding surface is composed only of friction and that the cohesion is zero [37]. The average internal friction angle of the discontinuity planes of Tawilah sandstone is 31° .

The slopes in the study area were divided into 6 classes according to their angle, and a slope angle map was produced by DEM (Figure 11), which shows that the ten stations are close to the wadi boundaries. Table 3 and Figure 12 summarize the slopes' attitude and structure, and the types, causes and probability of failures based on the field investigation and satellite image processing of these ten stations.

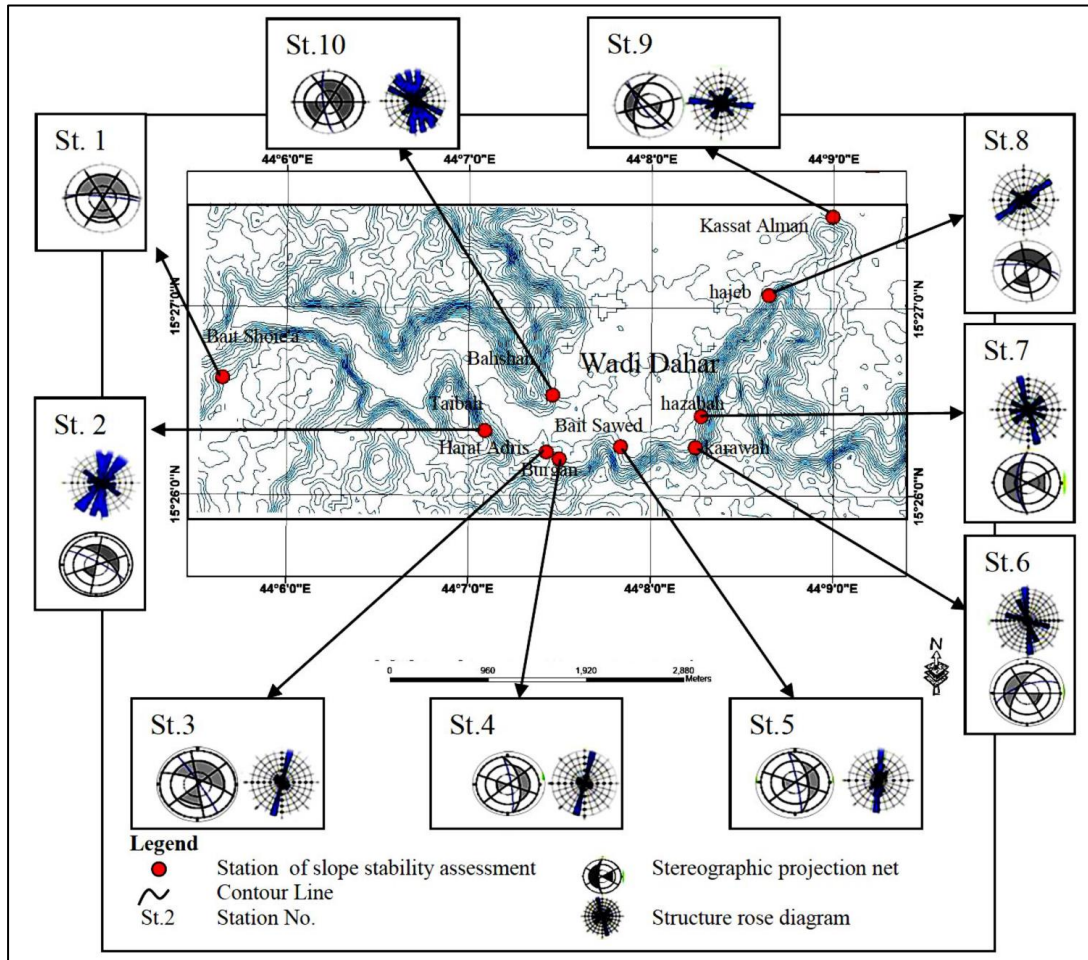


Figure 10. Topographic map showing the structure-slope failure relationship for the ten stations in the study area.

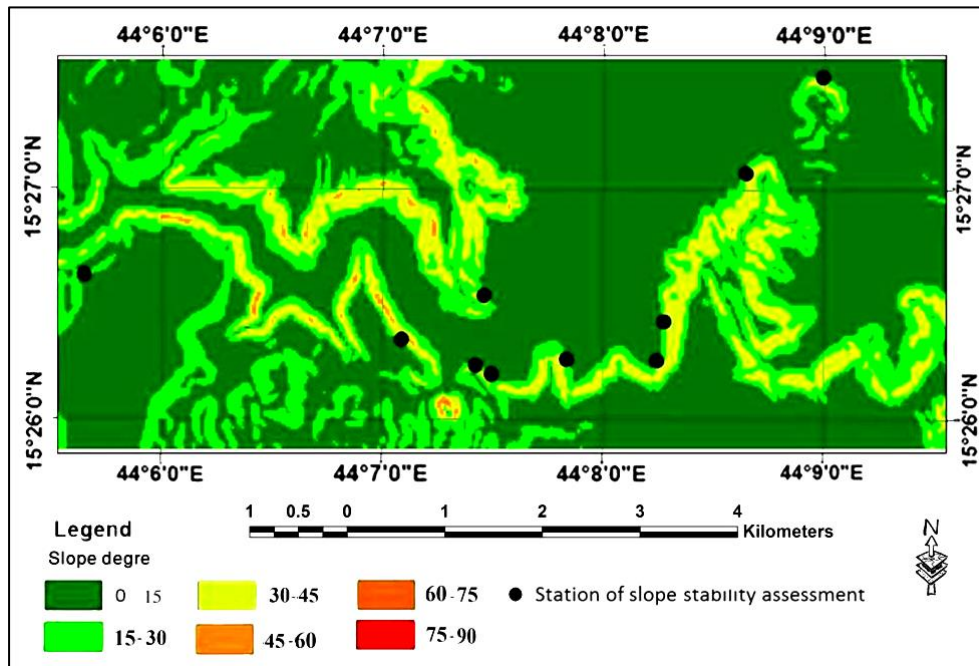


Figure 11. Digital elevation map showing the slope aspect at the study area and the location of the ten stations.

Table 3. Slope attitude, structure and failures at the ten stations at the study area, based on the field investigation and satellite image.

Station		Slope			Structure according to satellite image			Failure				
No.	Name	Altitude	Concordancy with the strata	No of discontinuities	Dominant trends	Second trend	Effective sets of joints (field measurements)	release surfaces	Type	Probability	Main causes	
1	Bait Shoie'a	000°/78°-OH	disconcordant	Not seen	--	--	the set of joints (005°/85°)	--	rockfall and secondary toppling	probable	differential weathering is the main cause of failure	
2	Tabah village	040°/62°-OH°	disconcordant	42	N-S and NE-SW	NW-SE	the secondary trend of joints (030°/80°)	the dominant trends	Plane sliding; rockfall and rolling	occurred and probable	differential weathering and presence of joints	
3	Harat Adris	020°/79°-OH°	disconcordant	7	NNE-SSW	NW-SE	the second set of joints (060°/86°)	the dominant trend	Plane sliding and rockfall	probable	differential weathering and presence of joints	
4	Burgan village	080°/58°-OH°	disconcordant	8	NNE-SSW	NW-SE	the second set of joints (080°/82°)	the dominant trend	Plane sliding; rockfall and rolling	probable	differential weathering; water infiltration and presence of joints	
5	Bait Sawed	080°/58°-OH°	disconcordant	8	N-S	NW-SE	the dominant set of joints (080°/82°)	the secondary trend	Plane sliding and rockfall	occurred and probable	differential weathering and presence of joints	
6	Karawah village	300°/65°-OH°	concordant	8	N-S and NNE-SSW	WNW-ESE	limited set of joint (340°/68°)	the dominant and second trends	Plane sliding rockfall and rolling	occurred and probable	differential weathering; water infiltration and presence of joints	
7	Hazabah village	270°/75°-OH°	concordant	7	NNE-SSW	NW-SE, NE-SW and E-W	the dominant set of joints (270°/65°)	the secondary trends	Plane sliding occurred	occurred and probable	differential weathering and presence of joints	
8	Hajeb village	285°/57°-OH°	concordant	17	E-W	NW-SE	the second set of joints (230°/75°)	the dominant trend	Plane sliding	occurred and probable	water infiltration, differential weathering and presence of joints	
9	Kassat Alman village	020°/70°-OH°	Disconcordant	64	NNW-SSE	NE-SW	the dominant set of joints (010°/75°)	the secondary trends	Toppling; rockfall and rolling	occurred and probable	water infiltration, weathering and presence of joints	
10	Bahshan village	020°/70°-OH°	Disconcordant	63	N-S and NNW-SSE	NE-SW	the dominant sets of joints (260°/78°)	the secondary trends	Plane sliding and rockfall	probable	water infiltration, weathering and presence of joints	

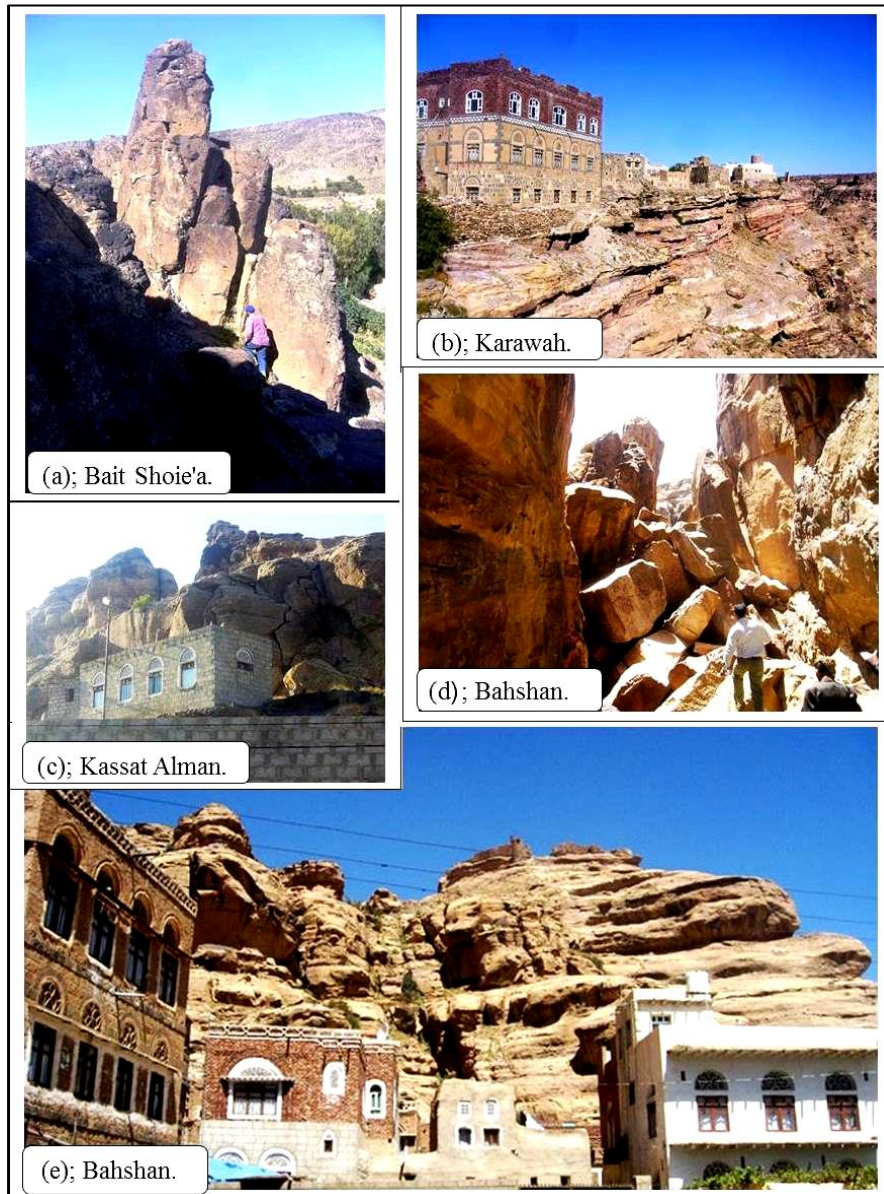


Figure 12. Selected Photos for different stations at the study area; a) probable toppling failure along basaltic rock at Bait Shoie'a station, b) differential weathering at Karawah station, c) the overhanging slope and the probable rockfall within it at Kassat Alman station, d) previous rockfall at Bahshan station and, e) the overhanging slope and the probable rockfall within it at Bahshan village.

7.2 Landslide Possibility Index Assessment

In the area under investigation about 95 out of 152 stations are located at rock outcrops, whereas the other 57 are at semi plane soil surfaces. The distance between stations ranges between 200 and 500 m to the northward and eastward coordinates (see Figure 1).

Based on the LPI assessment system several plots were created using Microsoft Excel (Figure 13) to show the relationship between the susceptibility category (LPI value) and the different affected features recognized, showing the correlation coefficient (R^2) for each relation. The LPI shows good correlation coefficient values with the orientation of the discontinuities ($R^2 = 0.94$), and with slope height ($R^2 = 0.88$) and slope angle ($R^2 = 0.85$) at linear equations (Figure 13a, b and c), that refer to the direct link of the slope.

On the other hand, poor correlations were found with the other factors such as grade of weathering ($R^2 = 0.02$) (Figure 13d). This might reflect the wide spread horizontal and gentle slopes of the exposed outcrops within the study area.

The above relationships prove that the LPI in the Wadi Dhahr area is mainly controlled by the factors of orientation of the discontinuities, slope height and slope angle. Digital maps were created using ArcGIS 9.3 to show the similarity of these factors (Figure 14a, b and c), and the dissimilarity of the other factors i.e. spacing of discontinuities (Figure 14d) with the final LPI value (Figure 14e).

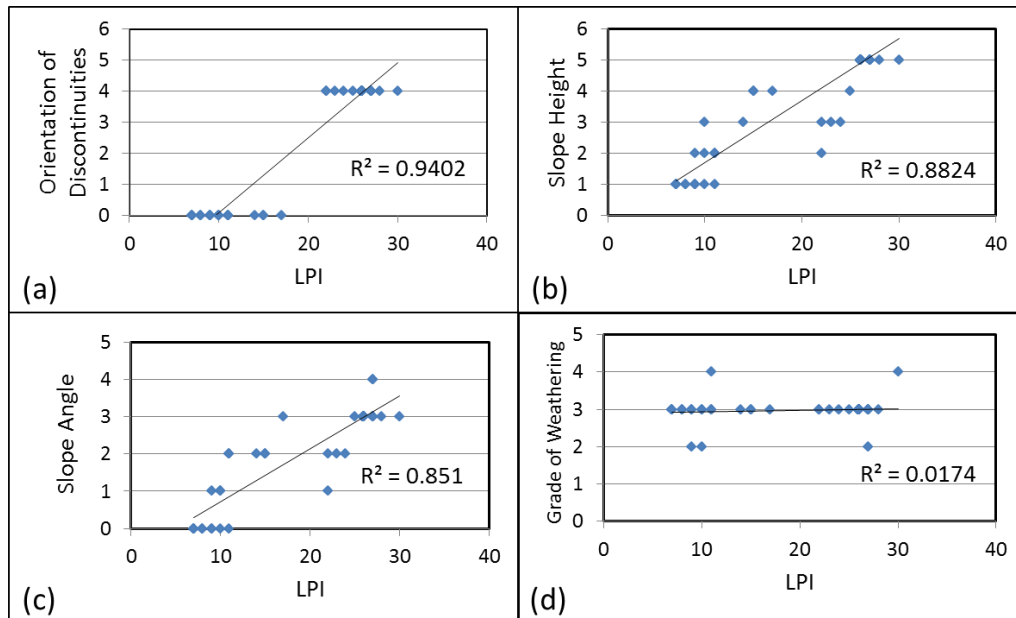


Figure 13. Graphic Relationships for rock formations representing the correlation values (R^2), between LPI and, a) orientation of discontinuities, b) slope height, c) slope angle, d) grade of weathering, in the studied area.

7.3 Landslide susceptibility map

The LPI rating system was divided to six classes, and the landslide susceptibility classified to six categories based on the LPI values. The number and percentage of each susceptibility category was calculated (Table 4). High and very high susceptibility zones cover 50% of the total study area and include 81% of the rock formations. Moderate susceptibility zones cover 38% of the total study area and include 07% of the rock formations, while low susceptibility zones and rock formations each cover 12% of the total study area (Figures 15a and b).

Based on the evaluation of landslide susceptibility categories in the study area, a digital landslide susceptibility map was created (Figure 16). This susceptibility map shows that the municipal regions lie under moderately and high susceptibility zones.

The discontinuities work as the main factor for failures [34, 38, 36, 39]. The ten studied stations show that the joints affecting failures measured by field investigation are in concordance with the dominant trend of joints recorded by image at 5 stations, and with the second trend of joints at 3 stations, and not in concordance at 2 stations. Plain sliding and rockfall are common features in the study area, each accounting for 36.4% of failures, while rolling (18.1%) and toppling (09.1%) are rare (Table 5). Secondary toppling [34] occurs if toe cutting by differential weathering and seasonal rainfall and runoff continues.

The main causes of failure are differential weathering (which produces mechanically complex failure [38]), discontinuities and rainfall, in that order of frequency (Table 5). The landslide susceptibility map (Figure 16) shows that seven of the ten stations lie at moderately high and high susceptibility zones.

7.4 Mitigation

It is necessary to take those construction measures most appropriate for the topographical, geological and operational conditions at the site to manage the problem of instability of the slopes [36]. The following treatments may achieve where they are needed:

- 1- Removal of rock overhang and unstable blocks by trim blasting
- 2- Removal of trees with roots growing in cracks
- 3- Support of the toe of the slope and of the overhanging parts by retaining walls.
- 4- Erecting well sealed drainage conduits.
- 5- Shotcrete grouting and grouting of discontinuities with a convenient filling material like cement, in order to increase the cohesion of the different parts of the rock mass, and to prevent water infiltration to the lower part of the slope.

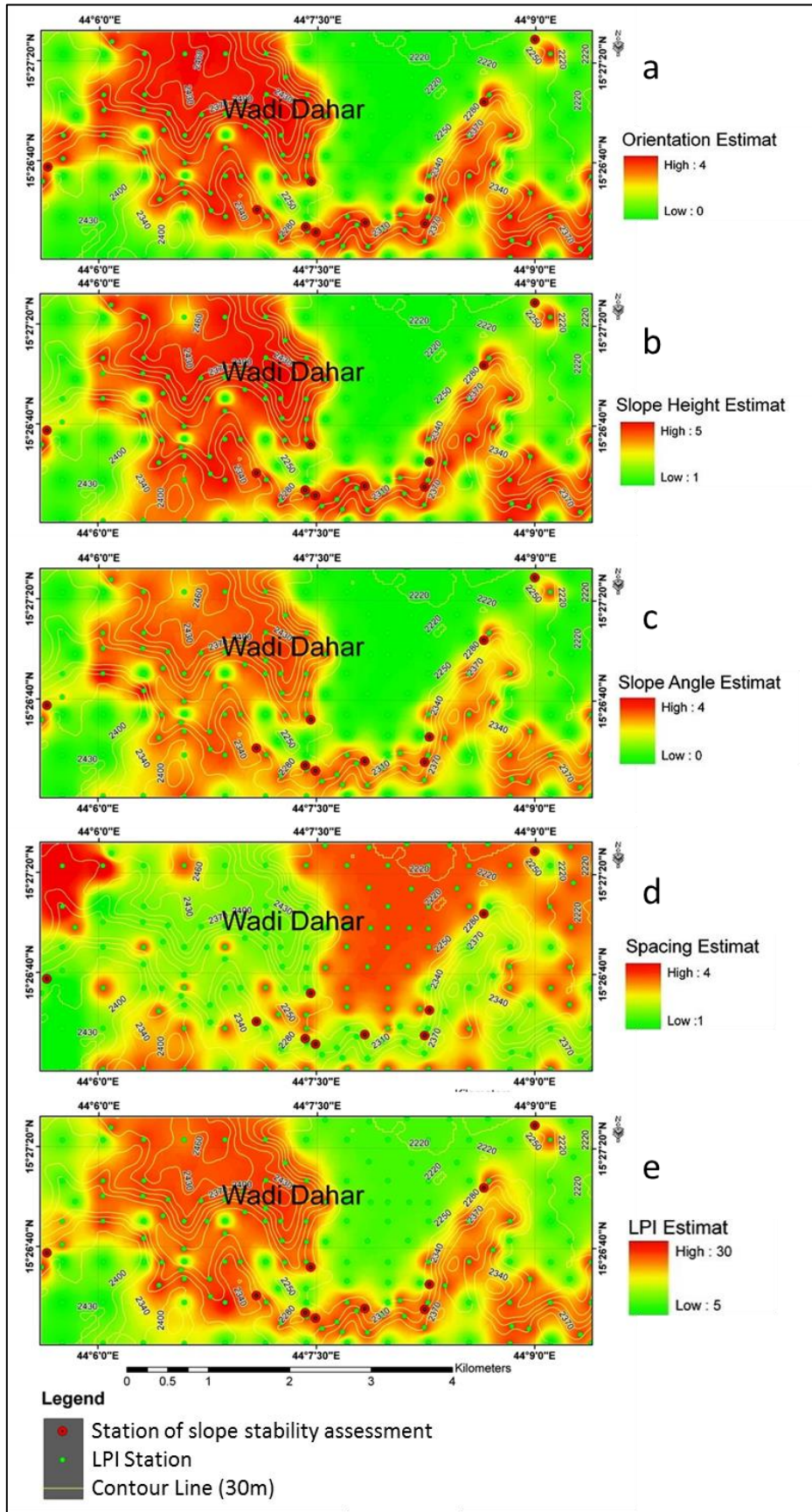


Figure 14. Digital maps of the study area based on the LPI chart, illustrating the distribution of values of different factors: a) orientation of the discontinuities, b) slope height, c) slope angle, d) spacing of discontinuities and e) final LPI.

SLOPE STABILITY ASSESSMENT AND LANDSLIDE SUSCEPTIBILITY MAP PRODUCTION

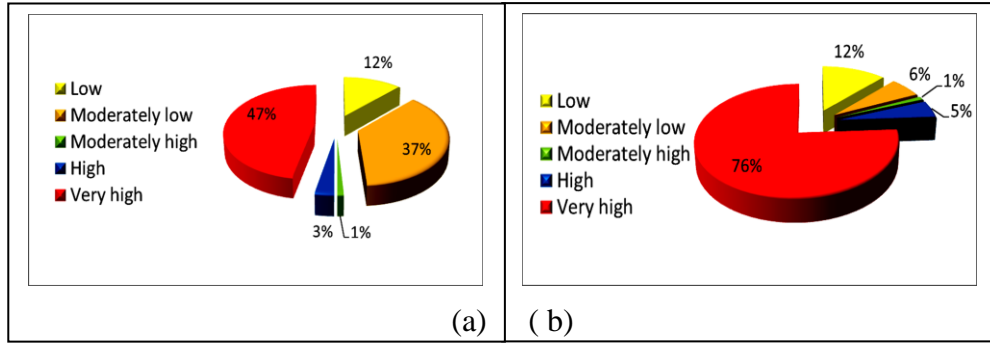


Figure 15. Percentages for the susceptibility categories at the study area; a) for rock and soil stations and, b) for rock formations only.

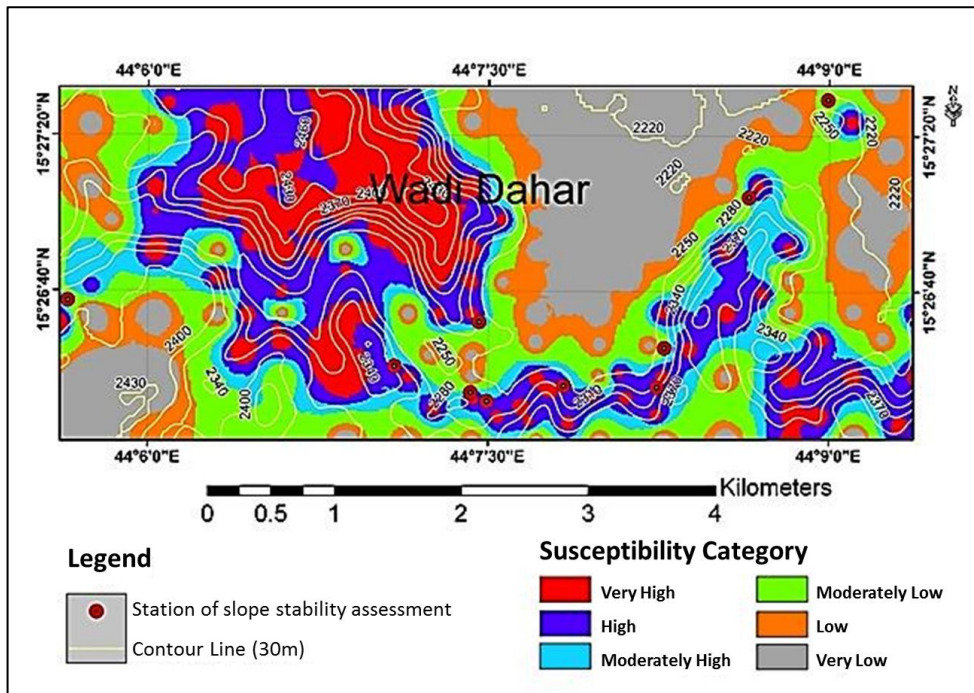


Figure 16. Landslide susceptibility map for the study area.

Table 4. Number and percentage of stations for LPI classes and the susceptibility categories for all stations and the area for rock formation.

LPI value	LPI class	susceptibility category	LPI for total study area (Rock and Soil)		LPI for Rock Formation	
			Number of stations	Percentage of susceptibility category	Number of stations	Percentage of susceptibility category
0 – 5	I	Very low	-	-		
6 – 10	II	Low	18	12 %	11	12%
11 – 15	III	Moderately low	56	37 %	6	6%
16 – 20	IV	Moderately high	1	01 %	1	1%
21 – 25	V	High	5	03 %	5	5%
> 25	VI	Very high	72	47 %	72	76%
Total			152	100 %	95	100 %

Table 5. Number and percentage of failure types and causes in the study area.

St. No.	Location	Type of failure				The main causes of failure		
		Rockfall	Plane sliding	Toppling	Rolling	differential weathering	Discontinuities	Rainfall
1	Bait Shoie'a	*		*		*		
2	Taibah village	*	*		*	*	*	
3	Harat Adris	*	*			*	*	
4	Burgan village	*	*		*	*	*	*
5	Bait Sawed	*	*			*	*	
6	Karawah village	*	*		*	*	*	*
7	Hazabah village		*			*	*	
8	Hajeb village		*			*	*	*
9	Kassat Alman village	*		*	*	*	*	*
10	Bahshan village	*	*			*	*	*
Total		8	8	2	4	10	9	5
Percentage		36.4 %	36.4 %	09.1 %	18.1 %	41.7 %	37.5 %	20.8 %

8. Conclusion

- 1- 2990 fractures have been recorded, 54.5% of them less than 20 m apart.
- 2- Fracture density is concentrated in the center, northern and eastern parts of the study area, especially in Tawilah sandstone outcrops and the slopes.
- 3- The dominant trend of the fractures is from NW-SE to NE-SW direction while the minimum trend is in an E-W direction.
- 4- The discontinuities recorded by satellite image are in concordance with field investigation for joints affecting failure at 8 stations and not concordance at 2 stations.
- 5- The LPI in the Wadi Dhahr area is mainly determined by the orientation of the discontinuities, slope height and slope angle factors.
- 6- Plane sliding and rockfall are the main modes of failure occurring in the area, with limited rolling and little toppling.
- 7- The main causes of failure are differential weathering, discontinuities and rainfall.
- 8- High and very high susceptibility zones cover half of the studied area.
- 9- Treatments are achievable for unstable slopes.
- 10- The results of this study will assist in slope management and land use planning in the area.

Acknowledgement

The field work for this study was partially funded by the Geological Survey and Mineral Resources Board of Yemen (G.S.M.R.B). The satellite images were provided by Yemen Remote Sensing and GIS Centre (YRSC).

References

1. Evans, S.G., Mugnozza, G.S., Strom, A., Hermanns, R.L. and Ischuk, A.V. Landslide From Massive Rock Slope Failure and Associated Phenomena. Springer. Printed in the Netherlands, 2006a, 3–52.
2. Evans, S.G., Mugnozza, G.S., Strom, A. and Hermanns, R.L. Landslides from Massive Rock Slope Failure. IV. *Earth and Environmental Science*. Springer. Printed in the Netherlands, 2006b, **49**: 662.
3. Brabb, E.E. Innovative approaches to landslide hazard and risk mapping. Proceedings of the Fourth International Symposium on Landslides, Canadian Geotechnical Society, Toronto, Canada, 16–21 September, 1984, **1**, 307–324,

SLOPE STABILITY ASSESSMENT AND LANDSLIDE SUSCEPTIBILITY MAP PRODUCTION

4. Tseng, C.M., Lin, C.W. and Hsieh, W.D. Landslide susceptibility analysis by means of event-based multi-temporal landslide inventories. *Natural Hazards and Earth System Sciences Journal*, European Geo sciences Union, 2015, **3**, 1137–1173.
5. Tazik, E., Jahantab, Z, Bakhtiari, M., Rezaei A. and Alavipanah, S.K. Landslide susceptibility mapping by combining the three methods Fuzzy Logic, Frequency Ratio and Analytical Hierarchy Process in Dozain basin. The 1st International Society of Photogrammetry and Remote Sensing (ISPRS) International Conference on Geospatial Information Research, Tehran, Iran, (2014), **XL(2/W3)**, 267-272.
6. Persichillo, M.G., Meisina, M.B., Bartelletti, C., Barsanti, M., Giannecchini, R., Avanzi, G.D., Galanti, Y. Cevasco, A., Brandolini, P. and Galve, J.P. Shallow landslides susceptibility assessment in different environments. *Geomatics, Natural Hazards and Risk Journal*, 2017, **8(2)**, 748–771.
7. Fell, R., Corominas, J., Bonnard, C., Cascini, L., Leroi, E. and Savage, W.Z. Guidelines for landslide susceptibility, hazard and risk zoning for land use planning. *Engineering Geology Journal*. 2008, **102**, 85- 98.
8. Kanwal, S., Atif, S. and Shafiq, M., GIS based landslide susceptibility mapping of northern areas of Pakistan, a case study of Shigar and Shyok Basins, *Geomatics, Natural Hazards and Risk Journal*, 2017, **8(2)**, 348-366.
9. Burns, W.J., Madin, I.P. and Mickelson, K.A. Protocol for Shallow-Landslide Susceptibility Mapping, Special Paper 45, Oregon Department of Geology and Mineral Industries. Nature of the Northwest Information Center, Portland, State of Oregon, 2012, 32p.
10. Corominas, J., Van Westen, C., Frattini, P., Cascini, L., Malet, J., Fotopoulou, S., Catani, F., Van Den Eeckhaut, M., Mavrouli, O. and Agliardi, F., Pitolakis, K., Winter, M.G., Pastor, M., Ferlisi, S., Tofani, V., Herva's, J. and Smith, J.T. Recommendations for the quantitative analysis of landslide risk. *Bulletin of Engineering Geology and the Environment*. 2014, **3**, 209–263.
11. Saha, A.K. An approach for GIS-based statistical landslide susceptibility zonation with a case study in the Himalayas. *Landslides Journal*, 2005, **2**, 61–69.
12. Van Westen, C.J., Castellanos, E. and Kuriakose, S.L. Spatial data for landslide susceptibility, hazard, and vulnerability assessment: an overview. *Engineering Geology Journal*, 2008, **102(3-4)**, 112–131.
13. Gupta, R.P., Kanungo, D.P., Arora, M.K. and Sarkar, S., Approaches for comparative evaluation of raster GIS-based landslide susceptibility zonation maps. *International Journal of Applied Earth Observation and Geoinformation*. 2008, **10(3)**, 330–341.
14. Civil Aviation and Meteorological Authority, Climatic Data, Station Sana'a. Computer Department, (2017), Sana'a, Yemen.
15. Davison, I., Al-Kadasi, M., Al-Khirbash, S., Al-Subbary, A.K., Baker, J., Blakey, S., Bosence, D., Dart, C., Heaton, R., McClay, K., Menzies, M., Nicols, G., Owen, L., Yelland, A. Geological evolution of the southeastern Red Sea rift margin, Republic of Yemen. *Geological Society Of America Bulletin*. 1994, **106**, 1474–1493
16. Heikal, M., Al-Khirbash, S., Hassan, A., Al-Kotbah, A., Al-Selwi, K., Lithostratigraphy, deformation history, and tectonic evolution of the basement rocks, Republic of Yemen: an overview. *Arabian Journal of Geosciences, Saudi Society for Geosciences*. 2014, **7 (5)**, 2007–2018.
17. Al-Subbary, A., Hamimi, Z., and Al-Kottbah, A., Tectono-sedimentary framework of the Cretaceous-Early Tertiary Tawilah Group, Wadi Dhahr district, Republic of Yemen. *Egyptian Journal of Geology*, 1999, **43/2**, 219-235.
18. Khanbari, K.M. Using remote sensing, GIS and field data for fracture analysis Wadi Dhar area, Republic of Yemen. *Faculty of Science Bulletin*, Sana'a University, Yemen, (2004), **17**, 91-102.
19. Menzies, M., Baker, J., Chazot, G., Al-Kadasi, M. Evolution of the Red sea volcanic margin, western Yemen. In: Large igneous provinces: continental, oceanic and planetary flood volcanism. *Geophysical Monograph*. 100, *American Geophysical Union*, 1997, 29–43.
20. Khanbari, K., and Huchon, P. Paleostress analysis of the volcanic margins of Yemen. *Arabian Journal of Geosciences*, (2010), **3**, 529–538.
21. Khanbari, K. Structural Analysis and Tertiary Tectonic Evolution of Yemen. *Faculty of Science Bulletin*, Sana'a University, Yemen. 2015, **27**, 75-87.
22. Huchon, P., Jestin, F., Cantagrel, J.M., Gaulier, J.M., Al Khirbash, S., and Gafaneh, A. Extension deformation in Yemen since Oligocene and the Afar triple junction. *Annales Tectonicae*, 1991, **5 (2)**, 141-163.
23. Al-Ubaidi, M.R., and Al-Kotbah, A.M. The magnitudes of the paleostresses of Yemen faults in sedimentary cover. *Faculty of Science Bulletin*., 2003, **16**, 95-109.
24. Gemitzi, A., Falalakis, G., Eskioglou, P., and Petalas, C. Evaluating Landslide susceptibility Using Environmental Factors, Fuzzy Membership Functions and GIS. *Global Network of Environmental Science and Technology Journal*, Greece. 2011, **13(1)**, 28-40.
25. Francipane A., Arnone, E., Lo Conti, F., Puglisi, C. and Noto, L.V. A Comparison Between Heuristic, Statistical, And Data-Driven Methods In Landslide Susceptibility Assessment: An Application To The Briga And Giampileri Catchments. *International Conference on Hydroinformatics*, City University of New York, 2014, 8p.
26. Bejerman, N.J. Evaluation of landslide susceptibility along State Road 5, Cordoba, Argentina. Proceedings, 8th International Congress of IAEG Vancouver, Canada, Balkema, Rotterdam, 1998, **2**, 1175-1178.
27. Barahim, A.A. *Slope Stability Study Of Hajja-Amran Road In Yemen And Derivation Of Toppling Equations For Blocks Having Triangular Cross-Section*. Unpublished PhD theses, Baghdad University, Iraq, 2004, 158.
28. Saaty, T.L. *The Analytical Hierarchy Process*, McGraw Hill, New York, 1980, 287.

29. Saaty, T.L. and Vargas, G.L. *Prediction, Projection and Forecasting*. Kluwer Academic Publishers, Dordrecht, 1991, 251.
 30. Saaty, T.L. and Vargas, G.L. *Models, Methods, Concepts, and Applications of the Analytic Hierarchy Process*. Kluwer Academic Publisher, Boston, 2001.
 31. Pour, A.B. and Hashim, M., Application of Landsat-8 and ALOS-2 data for structural and landslide hazard mapping in Kelantan, Malaysia. *Natural Hazards and Earth System Sciences, Copernicus Publications on behalf of the European Geosciences Union* 2017, **17**, 1285–1303,
 32. Anon: The preparation of Maps and Plans in Terms of Engineering Geology. *Quarterly Journal of Engineering Geology*. 1972, **5(4)**, 293-382.
 33. Al-Saadi, S.N. *A Method for Mapping Unstable Slopes with Reference to the Coastline of S.W. Dyfed, Wales*. Unpublished. PhD. Thesis, University of Bristol. 1981, 252.
 34. Hoek, E. and Bray, J.W. *Rock Slope Engineering*. (3rd Edition), Institution of Mining and Metallurgy, London, (1984), 358.
 35. Goodman, R.E. *Introduction to rock mechanics*. Wiley, New York. 1989, 478.
 36. Wyllie, D.C. and Mah, C.W. *Rock Slope Engineering Civil and Mining* (4th Edition), Taylor & Francis e-Library, 2004, 431.
 37. Karaman, K., Ercikdi, B. and Kesimal A. The assessment of slope stability and rock excavatability in a limestone quarry. *Earth Science Research Journal*, Universidad nacional De Colombia. 2013, **17 (2)**, 169 – 181.
 38. Evans, R.S. An Analysis of Secondary Toppling Rock Failures-the Stress redistribution Method. *Quarterly Journal of Engineering Geology*. 1981, **14**, 77-86.
 39. Sarkar, S., Kanungo, D.P. and Sharma, S. Landslide hazard assessment in the upper Alaknanda valley of Indian Himalayas. *Geomatics, Natural Hazards and Risk Journal*, 2013, **6(4)**, 308–325.
-

Received 10 December 2017

Accepted 6 May 2018